The impact of dust on the scaling properties of galaxy clusters

A. da Silva[1,2]⋆; A. Catalano[3], L. Montier[4], E. Pointecouteau[4], J. Lanoux[4], M. Giard[4]

[1] *Centro de Astrofisica da Universidade do Porto, Rua das Estrelas, 4150-762 Porto, Portugal*
[2] *Institut d'Astrophysique Spatiale, Bat 121, Universite Paris Sud, 91405 Orsay, France*
[3] *Observatoire de Paris - LERMA, 61 avenue de l'Observatoire, 75014 Paris, France*
[4] *CESR, CNRS - Université de Toulouse, BP 44346, F 31028, Toulouse cedex 04, France*

17 August 2008

ABSTRACT
We investigate the effect of dust on the scaling properties of galaxy clusters based on hydrodynamic N-body simulations of structure formation. We have simulated five dust models plus a radiative cooling and adiabatic models using the same initial conditions for all runs. The numerical implementation of dust was based on the analytical computations of Montier & Giard (2004). We set up dust simulations to cover different combinations of dust parameters that put in evidence the effects of size and abundance of dust grains. Comparing our radiative *plus* dust cooling runs to a purely radiative cooling simulation we find that dust has an impact on cluster scaling relations. It mainly affects the normalisation of the scalings (and their evolution), whereas it introduces no significant differences on their slopes. The strength of the effect critically depends on the dust abundance and grain size parameters as well as on the cluster scaling. Indeed, cooling due to dust is effective at the cluster regime and has a stronger effect on the "baryon driven" statistical properties of clusters such as $L_\mathrm{X} - M$, $Y - M$, $S - M$ scaling relations. Major differences, relative to the radiative cooling model, are as high as 25% for the $L_\mathrm{X} - M$ normalisation, and about 10% for the $Y - M$ and $S - M$ normalisations at redshift zero. On the other hand, we find that dust has almost no impact on the "dark matter driven" $T_\mathrm{mw} - M$ scaling relation. The effects are found to be dependent in equal parts on both dust abundances and grain sizes distributions for the scalings investigated in this paper. Higher dust abundances and smaller grain sizes cause larger departures from the radiative cooling (i.e. with no dust) model.

Key words: cosmology, galaxies: clusters, methods: numerical

1 INTRODUCTION

From the first stages of star and galaxy formation, non-gravitational processes drive together with gravitation the formation and the evolution of structures. The complex physics they involve rule the baryonic component within clusters of galaxies, and in a more general context within the intergalactic medium (IGM hereafter – see the review by Voit (2005) and references therein). The study of these processes is the key to our understanding of the formation and the evolution of large-scale structure of the Universe. Indeed, understanding how their heating and cooling abilities affect the thermodynamics of the IGM at large scales and high redshifts, and thus that of the intra-cluster medium (hereafter ICM) once the gas get accreted onto massive halos is a major question still to be answered. The continu-ous accretion and the merger events through which a halo assembled lead to a constant interaction of the IGM gas with the evolving galactic component. Within denser environments, like clusters, feedback provided by AGN balances the gas cooling (see for instance Cattaneo & Teyssier (2007); Conroy & Ostriker (2007), and McNamara & Nulsen (2007) for a review). Also, from high redshift, the rate of supernovae drives the strength of the galactic winds and thus the amount of material that ends ejected within the IGM and the ICM (see Loewenstein (2006)). These ejecta are then mixed in the environment by the action of the surrounding gravitational potential and the dynamics of cluster galaxies within.

Since long, X-ray observations have shown the abundant presence of heavy elements within the ICM (see for instance review works by (Sarazin 1988; Arnaud 2005)). Physical processes like ram-pressure stripping, AGN interaction with the ICM, galaxy-galaxy interaction or mergers are scrutinized

⋆ E-mail: asilva@astro.up.pt

within analytical models and numerical simulations in order to explain the presence of metals (see for instance works by (Kapferer et al. 2006; Domainko et al. 2006; Moll et al. 2007)). Moreover, it is obvious that the process of tearing of material from galaxies leads not only to the enrichment of the ICM/IGM in metal, but in gas, stars and dust as well. Recent work on numerical simulations (Murante et al. 2004, 2007; Conroy & Ostriker 2007) have stressed the role of hierarchical buiding of structures in enriching the ICM with stars in a consistent way with the observed amount of ICM globular clusters, and ICM light. Indeed, the overall light coming from stars in between cluster galaxies represent an important fraction of the total cluster light: for instance (Krick & Bernstein 2007) measured 6 to 22% from a sample of 10 clusters. The effect of a diffuse dust component within the IGM/ICM, and its effect is less known. A few observational studies with the ISO and the Spitzer satellites have tried without frank success to detect the signature of such a component (Stickel et al. 1998, 2002; Bai et al. 2006, 2007). More successfully, (Montier & Giard 2005) have obtained a statistical detection, via a stacking analysis, of the overall infrared emission coming from clusters of galaxies. However, they were not able to disentangle the IR signal from dusty cluster galaxies from a possible ICM dust component. On the other hand, from a theoretical point of view a few works have looked at the effect of dust on the ICM (Popescu et al. 2000) or in conjunction with the enrichment of the ICM in metals (Aguirre et al. 2001). However, the effect of dust on a ICM/IGM-type thermalized plasma has been formalized by (Montier & Giard 2004). These authors have computed the cooling function of dust taking into account the energetic budget for dust. They have shown the ability of dust to be a non negligible cooling/heating vector depending on the physical properties of the environment.

Dust thus comes, within the ICM/IGM, as an added source of non-gravitational physics that can potentially influence the formation and the evolution of large scale structure in a significant way. Indeed, since redshift of $z \simeq 2 - 5$ during which the star formation activity reached its maximum in the cosmic history, large amounts of dust has been produced and thus ejected out of the galaxies due to violent galactic winds into the IGM (Springel & Hernquist 2003). As this material is then accreted by the forming halos, one can wonder about the impact produced by dust on the overall properties of clusters of galaxies once assembled and thermalized. In a hierarchical Universe, the population of clusters is self-similar, thus is expected to present well defined structural and scaling properties. However, to date, it is common knowledge that the observed properties deviate form the prediction by a purely gravitational model (see (Voit 2005; Arnaud 2005) for review works). It is thus important to address the issue of the impact of dust on the statistical properties of structures such as clusters of galaxies, the same way it is done for AGNs, supernovae, stripping or mergers.

In order to tackle this question, we have put into place the first N-body numerical simulations of hierarchical structure formation implementing the cooling effect of dust according to the dust nature and abundance. In this paper, we present the first results of this work focusing at the scale of galaxy clusters, and more specifically on their scaling properties. The paper is organized as follows: we start by pre-

senting the physical dust model and how it is implemented in the numerical simulation code. In Sec . 3, we describe the numerical simulations and the various runs (i.e. model) that have been tested. From these simulations our analysis concerns the galaxy cluster scale, and focus on the impact of the presence of dust on the scaling relation of clusters. In Sec. 4, we present our results on the $M - T$, the $S - T$, the $Y - T$ and the $L_X - T$ relations. The derived results are presented in Sec. 5 and discussed in Sec.6.

2   THE DUST MODEL

In our numerical simulations the implementation of the physical effect of dust grains is based on the computation by Montier & Giard (2004) of the dust heating/cooling function. In this work, we decided to limit our implementation to the dust cooling effect only. Indeed the goal of this paper is to study the effect of dust at the galaxy cluster scales. The heating by dust grains is mainly effective at low temperatures (i.e $T_e < 10^5$ K) and is a localised effect strongly dependent of the UV radiation field. Our numerical simulations (see Sec. 3 and 6.2) do not directly implement this level of physics.

Dust grains in a thermal plasma with $10^6 < T < 10^9$ K are destroyed by thermal sputtering, which efficiency was quantified by Draine & Salpeter (1979, see their Eq. 44). The sputtering time depends on the column density and on the grain size. For grain sizes ranging form $0.001\mu m$ to $0.5\mu m$, and an optically thin plasma ($n \sim 10^{-3}$ atom/cm^2), the dust lifetime spawns from 10^6 yr for small grains up to 10^9 yr for big grains. This lifetimes are therefore large enough for the cooling by dust in the IGM/ICM to be considered. Evidently, it is also strongly linked to the injection rate of dust, thus to the physical mechanism that can bring and spread dust in the IGM/ICM.

Our implementation of the dust cooling power is based on the model by (Montier & Giard 2004). We recall bellow the main aspects of this model and describe the practical implementation within the N-body simulations.

2.1   The dust cooling function

Dust grains within a thermal gas such as the ICM or the IGM can either be a heating or a cooling vector depending on the physical state of the surrounding gas and on the radiative environment. Heating can occur via the photo-electric effect if the stellar radiation field (stars and/or QSOs) is strong enough (Weingartner (2006) and references therein). Indeed, the binding energies of electrons in dust grains are small, thus allowing electrons to be more easily photo-detached than in the case of a free atom or a molecule. On the other hand, the cooling by dust occurs through re-radiation in the IR of the collisional energy deposited on grains by impinging free electrons of the ICM/IGM [1].

Montier & Giard (2004) have computed the balance of the heating and cooling by dust with respect to the dust abundance: cooling by dust dominates at high temperatures

---

[1] In the galactic medium the cooling occurs through re-radiation of the power absorbed in the UV and visible range.

in the hot IGM of virialized structures (i.e clusters of galaxies), and heating by dust dominates in low temperature plasma under high radiation fluxes such as in the proximity of quasars. The details, of course, depend on the local physical parameters such as the grain size and the gas density.

Assuming local thermal equilibrium for the dust, the overall balance between heating and cooling in dust grains can be written as follows:

$$\Lambda^g(a, T_d) = H^g_{coll}(a, T_e, n_e),\tag{1}$$

with H_{coll} being the collisional heating function of the grain and Λ the cooling function due to thermal radiation of dust. a is the grain size, T_e and n_e are respectively the electronic temperature and density of the medium and T_d is the dust grain temperature.

The heating of the dust grain was taken from Dwek (1981) and can be expressed in a general way as:

$$H^g_{coll}(a, T_e, n_e) \propto n_e\, a^\alpha\, T_e^\beta\tag{2}$$

where the values of α and β are dependent of the value of the ratio $a^{2/3}/T_e$.

The relevant dust parameters affecting the cooling function are the grain size and the metallicity. Indeed, the smaller the grains and the higher the metallicity, the higher is the cooling power of the dust. Thus the total cooling function due to a population of dust grains can be expressed as a function of these two parameters as:

$$\Lambda(a, T_d) = \int\int\int \Lambda^g(a, T_d)\frac{\mathrm{d}N(a, Z, V)}{\mathrm{d}V\mathrm{d}a\mathrm{d}Z}\mathrm{d}V\mathrm{d}a\mathrm{d}Z\tag{3}$$

where $\mathrm{d}N(a, Z, V)/\mathrm{d}V\mathrm{d}a\mathrm{d}Z$ is the differential number of dust grains per size, metallicity and volume element.

Cooling by dust happens to increase with the square root of the gas density, whereas the heating by dust is proportional to the density. As stressed by Montier & Giard (2004) the cooling by dust is more efficient within the temperature range of $10^6 < T < 10^8$ K (i.e $0.1 < kT < 10$ keV), which is typically the IGM and ICM thermal conditions.

We redirect the reader to Montier & Giard (2004) for a full description of the dust model, and a comprehensive physical analysis of the effect of dust in a optically thin plasma.

2.2   The dust abundance

The abundance of dust is a key ingredient to properly weight in our implementation. Observations indicate that dust represents only a tiny fraction of the baryonic matter: $M_{dust}/M_{gas} \approx 0.01$ in our Milky Way (Dwek et al. 1990), and this is possibly lower by a factor 100 to 1000 in the ICM: $M_{dust}/M_{gas} = 10^{-5} - 10^{-4}$ (Popescu et al. 2000; Aguirre et al. 2001). We defined the abundance of dust as the ratio of the dust mass with respect to the gas mass:

$$Z_d = \frac{M_{dust}}{M_{gas}} = f_d\, \frac{Z}{Z_\odot}\, Z_{d\,\odot}\tag{4}$$

where Z is the metallicity in units of solar metallicity, $Z_{d\,\odot} = 0.0075$ is the solar dust abundance, i.e the dust-to-gas mass ratio in the solar vincinity (Dwek et al. 1990), and f_d is the abundance of dust in the ICM in units of solar dust abundance.

Dust enrichment occurs via the feedback of galaxy formation and evolution in the ICM through interaction, stripping, mergers, galactic winds and AGNs outburst. At all redshifts, it is linked to the SFR which drives the production of dust in cluster galaxies. However, in our hydrodynamic simulations (see Sect. 3) the SFR is not physically modeled, but it is inferred by the cooling state of the gas particles within the simulations: gas particles below a given threshold of temperature and above a given threshold of density are considered as colisionless matter, forming stars and galaxies (see Sec. 3). In order to tackle this problem, we choose to directly link the dust abundance to the metal abundance using Eq. (4). Therefore, the dust distribution in our simulations mimics the metal distribution.

2.3   Implementation in the N-body simulations

From the equations presented in the previous sections, we computed the dust cooling function according to the embedding medium temperature and (global) metallicity. In simulations, once the metallicity and temperature are known, a and f_d are the only two parameters driving the dust cooling rate (i.e $\Lambda(a, Z) = \Lambda(a, f_d)$). In the top panel of Fig. 1 we present dust cooling rates (red lines) for $f_d = 0.1$ and $a = 10^{-3}$ μm (model D1, see below) at different values of metallicity. The blue and black lines are the radiative cooling rates from Sutherland & Dopita (1993) and the total (i.e radiative plus dust cooling) rate, respectively.

Together with an adiabatic run (i.e model A) and a "standard" radiative run (model C – see Sect. 3 for further details), we ran a total of five runs implementing various population of grains (i.e named D1 to D5) characterized by their sized and dust-to-metal mass ratio:

• We tested three types of sizes: two fixed grain sizes with $a = 10^{-3}$ μm and $a = 0.5$ μm), respectively labeled *small* and *big*. The third assumes for the IGM dust grains a distribution in sizes as defined by Mathis et al. (1977) for the galactic dust: $N(a) \propto a^{-3.5}$ within the size interval of $[0.001, 0.5]$ μm. It is hereafter referred as the 'MRN' distribution.

• We investigate three values of f_d: 0.001, 0.01 and 0.1. The two extreme values roughly bracket the current theoretical and observational constraints on dust abundance in the ICM/IGM (i.e $10.^{-5}$ and 10^{-3} in terms of dust-to-gas mass ratio) (Popescu et al. 2000; Aguirre et al. 2001; Chelouche et al. 2007; Muller et al. 2008; Giard et al. 2008).

Tab. 1 lists code names and simulation details of all runs used in this work. In case of models D1 to D5, simulation cooling rates are given by the added effect of cooling due to dust and radiative gas cooling. Total cooling functions are displayed (non-coloured lines) in the bottom panel of Fig 1 for each of these models at $Z/Z_\odot = 0.33$. As the Figure indicates, the effect of dust cooling is stronger for models with higher dust-to-metal mass abundance parameters, f_d, and for smaller grain sizes (model D1). For low values of f_d the impact of dust cooling is significantly reduced. For example, in the case of model D5, the contribution of dust to the total cooling rate is negligible at $Z/Z_\odot = 0.33$ for all temperatures. Therefore we do not expect to obtain significant differences between simulations with these two models.
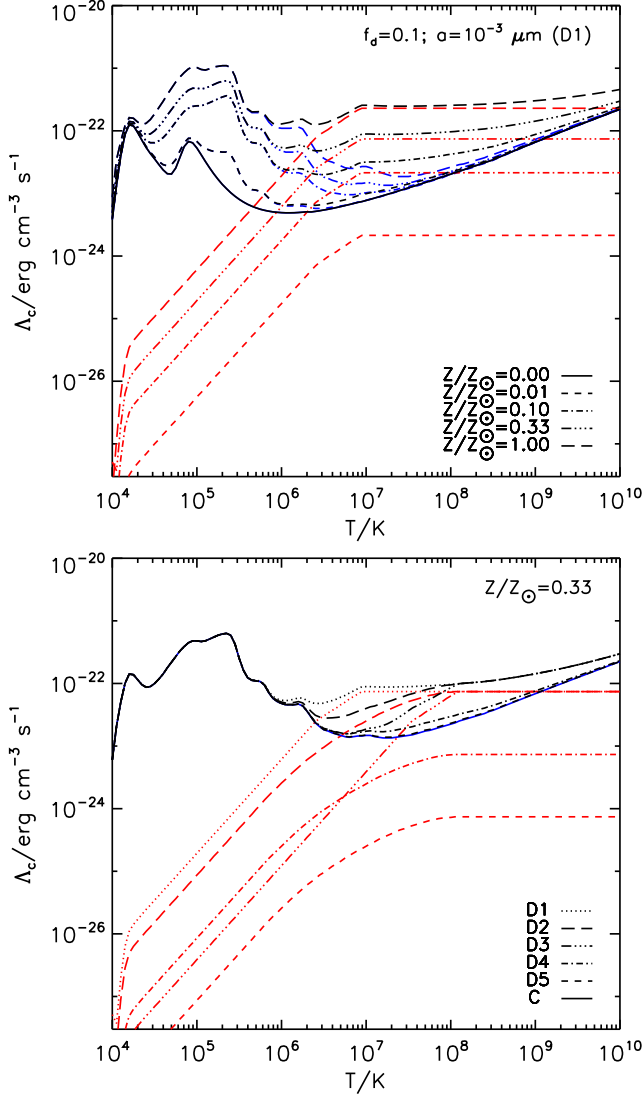
Figure 1. Cooling functions implemented in the numerical simulations. Top panel shows the dependence of dust model D1 ($f_d = 0.1$ and $a = 10^{-3}$ μm) with metallicity (and temperature) whereas the bottom panel shows different dust models at the same metallicity $Z/Z_\odot = 0.33$ (see text). Black, blue and red curves are the total cooling functions, radiative cooling of the gas from Sutherland & Dopita (1993) and dust cooling functions, respectively.

3   NUMERICAL SIMULATIONS

3.1   Simulation description

Simulations were carried out with the public code package `Hydra`, (Couchman et al. 1995; Pearce & Couchman 1997), an adaptive particle-particle/particle-mesh (AP^{3}M), (Couchman 1991) gravity solver with a formulation of smoothed particle hydrodynamics (SPH), see Thacker & Couchman (2000), that conserves both entropy and energy. In simulations with cooling gas particles are allowed to cool using the method described in Thomas & Couchman (1992) and the cooling rates presented in previous Section. At a given time step, gas particles with overdensities (relative to the critical density)

Run	Physics	f_d	Grain size	N_{steps}
A	adiabatic (no dust)	-	-	2569
C	cooling (no dust)	-	-	2633
D1	cooling with dust	0.100	small	2944
D2	cooling with dust	0.100	MRN	2920
D3	cooling with dust	0.100	big	2886
D4	cooling with dust	0.010	MRN	2698
D5	cooling with dust	0.001	MRN	2633

Table 1. Simulation parameters: f_d, dust-to-metal mass ratios (see Eq. 4), grain sizes, and number of timesteps taken by simulation runs to evolve from z=49 to z=0. Cosmological and simulation parameters were set the same in all simulation, as follows: $\Omega = 0.3$, $\Omega_\Lambda = 0.7$, $\Omega_b = 0.0486$, $\sigma_8 = 0.9$, $h = 0.7$, boxsize $L = 100\,h^{-1}$Mpc, and number of baryonic and dark mater particles, $N = 4,096,000$.

larger than 10^4, and temperatures below 1.2×10^4K are converted into collisionless baryonic matter and no longer participate in the gas dynamical processes. The gas metallicity is assumed to be a global quantity that evolves with time as $Z = 0.3(t/t_0)Z_\odot$, where $Z_\odot$ is the solar metallicity and t/t_0 is the age of the universe in units of the current time.

All simulations were generated from the same initial conditions snapshot, at $z = 49$. The initial density field was constructed, using $N = 4,096,000$ particles of baryonic and dark matter, perturbed from a regular grid of fixed comoving size $L = 100\,h^{-1}$Mpc. We assumed a Λ-CDM cosmology with parameters, $\Omega = 0.3$, $\Omega_\Lambda = 0.7$, $\Omega_b = 0.0486$, $\sigma_8 = 0.9$, $h = 0.7$. The amplitude of the matter power spectrum was normalized using $\sigma_8 = 0.9$. The matter power spectrum transfer function was computed using the BBKS formula (Bardeen et al. 1986), with a shape parameter Γ given by the formula in Sugiyama (1995). With this choice of parameters, the dark matter and baryon particle masses are $2.1 \times 10^{10}\,h^{-1}M_\odot$ and $2.6 \times 10^9\,h^{-1}$M$_\odot$ respectively. The gravitational softening in physical coordinates was $25\,h^{-1}$kpc below $z = 1$ and above this redshift scaled as $50(1+z)^{-1}\,h^{-1}$kpc.

We generate a total of 7 simulation runs, listed in Table 1. The first two runs, which will be referred hereafter as 'adiabatic' (or model 'A') and 'cooling' (or model 'C') simulations, do not include dust. Simulations 3 to 7 differ only on the dust model parameters assumed in each case, and will be referred to as 'dust' runs, and are labeled as 'D1' to 'D5' models (see Sec. 2.3 for details on the dust models definition). This will allow us to investigate the effects of the dust model parameters on our results. The last column in the table gives the total number of timesteps required by each simulation to arrive to redshift zero. For each run we stored a total of 78 snapshots in the redshift range $0 < z < 23.4$. Individual snapshots were dump at redshift intervals that correspond to the light travel time through the simulation box, ie simulation outputs stack in redshift.

3.2 Catalogue construction

Cluster catalogues are generated from simulations using a modified version of the Sussex extraction software developed by Thomas and collaborators (Thomas et al. 1998; Pearce et al. 2000; Muanwong et al. 2001). Briefly, the cluster identification process starts with the creation of a minimal-spanning tree of dark matter particles which is then split into clumps using a maximum linking length equal to $0.5 \, \Delta_{\mathrm{b}}^{-1/3}$ times the mean inter-particle separation. Here Δ_{b} the contrast predicted by the spherical collapse model of a virialized sphere (Eke, Navarro & Frenk 1998). A sphere is then grown around the densest dark matter particle in each clump until the enclosed mass verifies

$$M_\Delta (< R_\Delta) = \frac{4\pi}{3} R_\Delta^3 \, \Delta \, \rho_{\mathrm{crit}}(z). \tag{5}$$

where Δ is a fixed overdensity contrast, $\rho_{\mathrm{crit}}(z) = (3H_0^2/8\pi G)E^2(z)$ is the critical density and $E(z) = H(z)/H_0 = \sqrt{(\Omega(1+z)^3 + \Omega_\Lambda}$. Cluster properties are then computed in a sphere of radius R_{200}, ie with $\Delta = 200$, for all objects found with more than 500 particles of gas and dark matter. This means that our original catalogues are complete in mass down to $1.18 \times 10^{13} h^{-1} M_\odot$. For the study presented in this paper we have trimmed our original catalogues to exclude galaxy groups with masses below $M_{\mathrm{lim}} = 5 \times 10^{13} h^{-1} M_\odot$. In this way the less massive object considered in the analysis is resolved with a minimum of 2100 particles of both gas and dark mater. Our catalogues at z=0 have at least 60 clusters with masses above M_{lim}. This number drops to about 20 clusters at z=1.

Cluster properties investigated in this paper are the mass, M, mass-weighted temperature, T_{mw} and entropy, S (defined as $S = k_{\mathrm{B}} T / n^{-2/3}$), integrated Compton parameter, Y (i.e roughly the SZ signal times the square of the angular diameter distance to the cluster), and core excised (50 h^{-1}kpc) X-ray bolometric luminosity, L_{X}. These were computed in the catalogues according to their usual definitions, see da Silva et al. (2004):

$$M = \sum_k m_k, \tag{6}$$

$$T_{\mathrm{mw}} = \frac{\sum_i m_i \, T_i}{\sum_i m_i}, \tag{7}$$

$$S = \frac{\sum_i m_i \, k_{\mathrm{B}} T_i \, n_i^{2/3}}{\sum_i m_i}, \tag{8}$$

$$Y = \frac{k_{\mathrm{B}} \sigma_{\mathrm{T}}}{m_{\mathrm{e}} c^2} \frac{(1+X)}{2m_{\mathrm{H}}} \sum_i m_i \, T_i, \tag{9}$$

$$L_{\mathrm{X}} = \sum_i \frac{m_i \, \rho_i \, \Lambda_{\mathrm{bol}}(T_i, Z)}{(\mu m_{\mathrm{H}})^2}, \tag{10}$$

where summations with the index i are over hot ($T_i > 10^5$K) gas particles and the summation with the index k is over all (baryon and dark matter) particles within R_{200}. Hot gas is assumed fully ionised. The quantities m_i, T_i, n_i and ρ_i are the mass, temperature, number density and mass density of gas particles, respectively. Λ_{bol} is the bolometric cooling function in Sutherland & Dopita (1993) and Z is the gas metallicity. Other quantities are the Boltzmann constant, k_{B}, the Thomson cross-section, σ_{T}, the electron mass at rest,

m_{e}, the speed of light c, the Hydrogen mass fraction, $X = 0.76$, the gas mean molecular weight, μ, and the Hydrogen atom mass, m_{H}.

4 SCALING RELATIONS

In this paper we investigate the scalings of mass-weighted temperature, T_{mw}, entropy, S, integrated Compton parameter, Y and core excised X-ray bolometric luminosity, L_{X}, with mass, M. Taking into account Eq. (5) these cluster scaling relations can be expressed as:

$$T_{\mathrm{mw}} = A_{\mathrm{TM}} \left(M/M_0\right)^{\alpha_{\mathrm{TM}}} (1+z)^{\beta_{\mathrm{TM}}} E(z)^{2/3}, \tag{11}$$

$$S = A_{\mathrm{SM}} \left(M/M_0\right)^{\alpha_{\mathrm{YT}}} (1+z)^{\beta_{\mathrm{YT}}} E(z)^{-2/3}, \tag{12}$$

$$Y = A_{\mathrm{YT}} \left(M/M_0\right)^{\alpha_{\mathrm{YM}}} (1+z)^{\beta_{\mathrm{YM}}} E(z)^{2/5}, \tag{13}$$

$$L_{\mathrm{X}} = A_{\mathrm{LM}} \left(M/M_0\right)^{\alpha_{\mathrm{LM}}} (1+z)^{\beta_{\mathrm{LM}}} E(z)^{7/3}, \tag{14}$$

where $M_0 = 10^{14} h^{-1} M_\odot$ and the powers of the $E(z)$ give the predicted evolution, extrapolated from the self-similar model, (Kaiser 1986), of the scalings in each case. The quantities, A, α, and β, are the scalings normalisation at $z = 0$; the power on the independent variable; and the departures from the expected self similar evolution with redshift.

These scalings can be expressed in a condensate form,

$$y \, f(z) = y_0(z) \, (x/x_0)^\alpha, \tag{15}$$

where y and x are cluster properties (e.g. T_{mw}, M),

$$y_0(z) = A \, (1+z)^\beta, \tag{16}$$

and $f(z)$ is some fixed power of the cosmological factor $E(z)$. To determine A, α, and β for each scaling we use the method described in da Silva et al. (2004); Aghanim et al. (2008). To summarize, the method involves fitting the simulated cluster populations at each redshift with Eqs. (15) and (16) written in logarithmic form. First we fit the cluster distributions with a straight-line in logarithmic scale at all redshifts. If the logarithmic slope α remains approximately constant (i.e. shows no systematic variations) within the redshift range of interest, we then set α as the best fit value at $z = 0$. Next, we repeat the fitting procedure with α fixed to $\alpha(z = 0)$ to determine the scaling normalisation factors $y_0(z)$. This avoids unwanted correlations between α and $y_0(z)$. The r.m.s. dispersion of the fit is also computed at each redshift according to the formula,

$$\sigma_{\log y'} = \sqrt{\frac{1}{N} \sum_i (\log(y_i'/y'))^2}, \tag{17}$$

where $y' = yf$ (see Eq. (15)) and y_i' are individual data points. Finally, we perform a linear fit of the normalisation factors with redshift in logarithmic scale, see Eq. (16), to determine the parameters A and β.

We note that above $z = 1.5$ the number of clusters in our catalogues decreases typically below 10, hence, we do not fit the scaling relations above this redshift value.
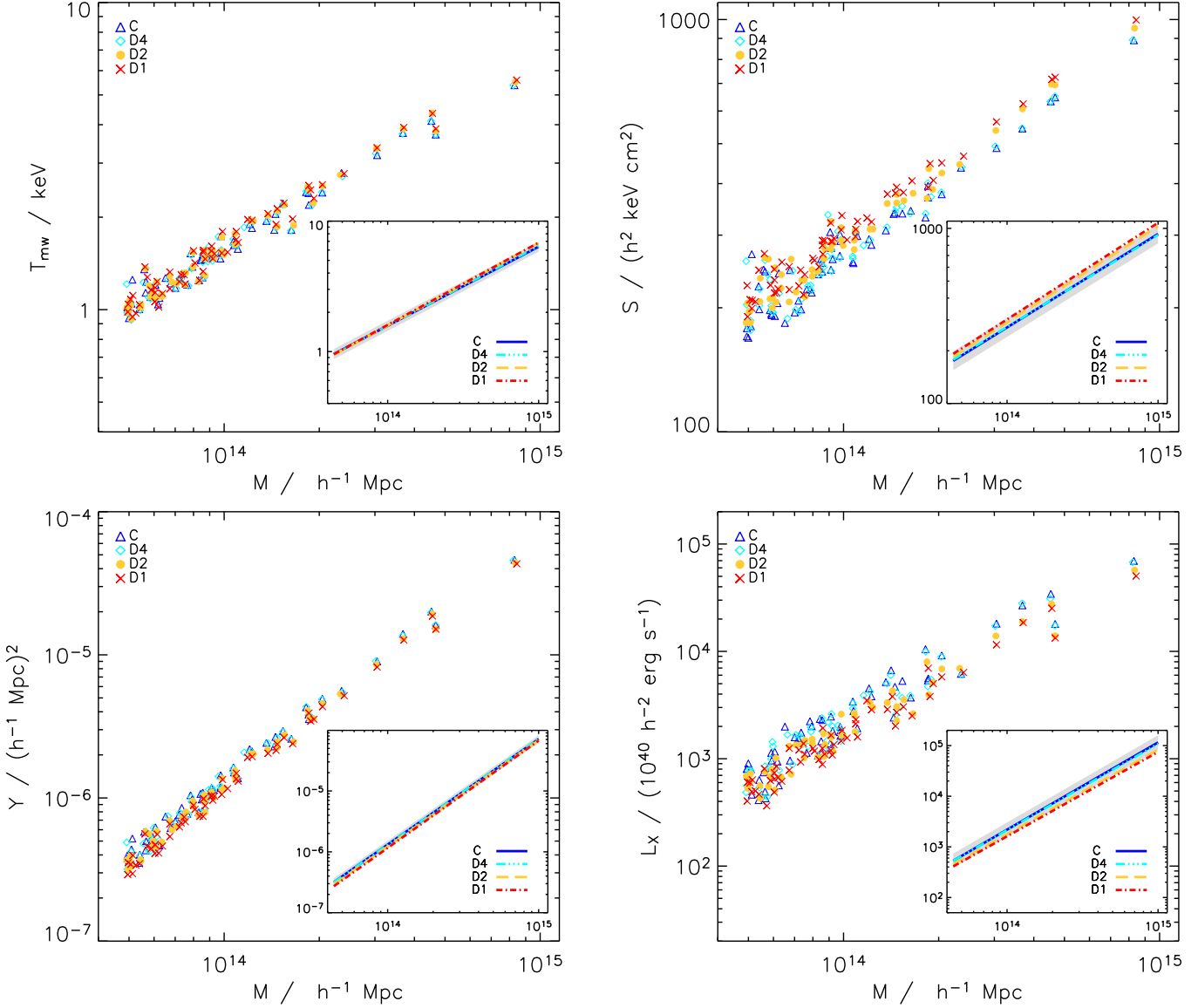
Figure 2. Cluster scalings at redshift zero for the $T_{\mathrm{mw}} - M$ (top left panel), $S - M$, (top right panel), $Y - M$ (bottom left panel), and $L_{\mathrm{X}} - M$ (bottom right panel). Displayed quantities are computed within R_{200}, the radius where the mean cluster density is 200 times larger than the critical density. Blue colour and triangles stand for the cooling (C) run, cyan and diamonds are for the D4 run, yellow and filled circles are for clusters in the D2 run, and red and crosses are for the D1 run. The lines in the embedded plots are the best-fit lines to the cluster distributions and the shaded areas are the fit r.m.s. dispersions for the C model, for each scaling.

5   RESULTS

5.1   Scaling relations at $z = 0$

In this section we present cluster scaling relations obtained from simulations at redshift zero. We investigate the four scalings presented in Section 4 for all models under investigation.

   Figure 2 shows the $T_{\mathrm{mw}} - M$ (top left panel), $S_{\mathrm{mw}} - M$, (top right panel), $Y - M$ (bottom left panel), and $L_{\mathrm{X}} - M$ (bottom right panel) scalings, with all quantities computed within R_{200}. In each case, the main plot shows the cluster distributions for the C (triangles), D4 (diamonds), D2 (filled circles) and D1 (crosses) simulations, whereas the embedded plot presents the power law best fit lines (solid, triple dot-dashed, dashed and dot-dashed for C, D4, D2 and D1

models, respectively) obtained in each case, colour coded in the same way as the cluster distributions. Here we have chosen to display dust models that allow us to assess the effect of dust parameters individually. For example, the dust models in runs D4 and D2 only differ by the dust-to-metal mass ratio parameter, whereas models D2 and D1 have different grain sizes but the same f_d. The shaded gray areas in the embedded plots give the r.m.s. dispersion of the fit for cooling (C) model. The dispersions obtained for the other models have similar amplitudes to the C case. The scalings of entropy and X-ray luminosity with mass show larger dispersions because they are more sensitive to the gas physical properties (density and temperature) in the inner parts of clusters than the mass-weighted temperature and Y versus mass relations which are tightly correlated with mass.

An inspection of Fig. 2 allows us to conclude that the cluster scalings laws studied here are sensitive to the underlaying dust model, and in particular to models where the dust cooling is stronger (model D1 and D2). The differences are more evident in the $S - M$ and $L_X - M$ scalings, but are also visible, to a lower extent, in the $T_{\mathrm{mw}} - M$ and $Y - M$ relations. Generally, the inclusion of dust tends to increase temperature and entropy because the additional cooling increases the formation of collisionless (star forming) material leaving the remaining particles in the gas phase with higher mean temperatures and entropies. The decrease of Y and X-ray luminosities reflects the effect of lowering the hot gas fraction and density due to dust cooling. These effects dominate over the effect of increasing the temperature.

In fact a closer inspection of Fig. 2 indicates that differences for the same cluster in different models (note that all simulations have the same initial conditions so a cluster-to-cluster comparison can be made), reflect the differences of intensity between cooling functions presented in Figure 1. For example, the differences between models D4 and C are clearly small as one would expect from the small differences between cooling functions displayed in the bottom panel of Figure 1. Another interesting example is that an increase of one order of magnitude in f_d from D4 to D2 seems to cause a stronger impact in the properties of the most massive clusters than the differences arising from changing the dust grain sizes from D2 to D1. Again this reflects the differences between cooling functions, which in the latter case are smaller at higher temperatures (see bottom panel of Figure 1).

A way of quantifying the effect of dust, is to look at the best fit slope, α, and normalisation, $\log A$, parameters of these scalings which are presented in Table 2 for all cooling models considered in this paper. We find that fitting parameters are quite similar for models C, D5, and D4 whereas models with high dust abundances provide the strongest variations of the fitting parameters, particularly for the normalisations. In several cases, differences are larger than the (statistical) best-fit errors, particularly for the D1 and D2 models. We also investigated scalings at redshift zero for the A (adiabatic) model and found they were consistent with self-similar predictions. As expected, the results obtained for the adiabatic and cooling models are in very good agreement with the findings of (da Silva et al. 2004; Aghanim et al. 2008) which use similar simulation parameters and cosmology.

5.2 Evolution of the scaling relations

We now turn to the discussion of the evolution of the cluster scaling laws in our simulations. Here we apply the fit to a power law procedure described in Section 4 to derive the logarithmic slope, β, of our fitting functions, Eqs. (11)-(14). As mentioned earlier, this quantity measures evolution departures relative to the self-similar expectations for each scaling.

In Figs. 3, 4, 5, and 6 we plot the redshift dependence of the power law slopes, α, (top panels), and normalisations, $\log y_0$, (middle panels) for our $T_{\mathrm{mw}} - M$, $S - M$, $Y - M$, and $L_X - M$ scalings, respectively. The bottom panels show straight lines best fits, up to z=1, to the data points in the middle panels of each Figure. The slopes of these lines are the β parameters in Eqs. (11)-(14). We decided not to in-
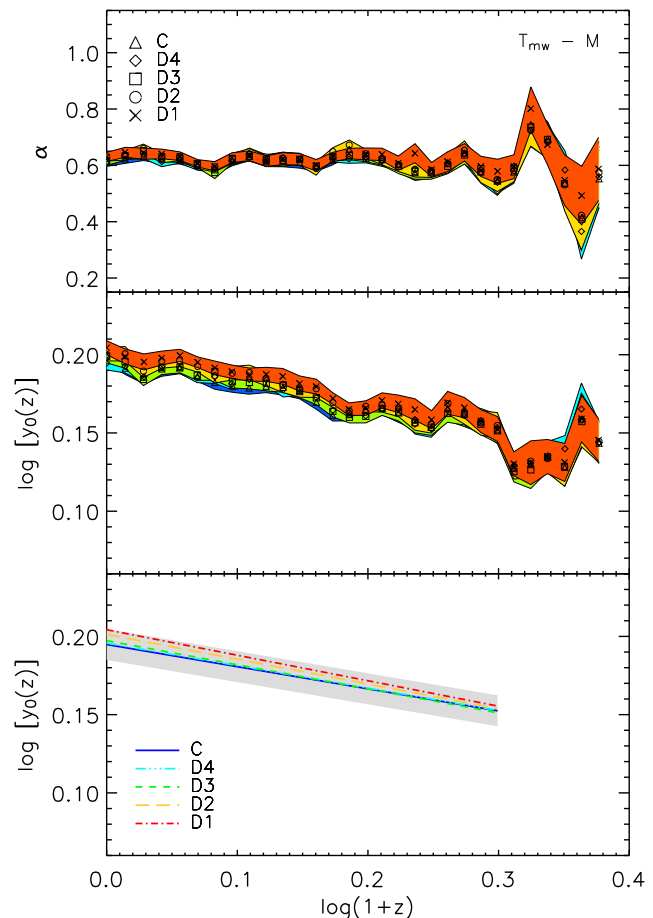

Figure 3. Evolution of the slope (top panel), normalisation (middle panel), and normalisation best fit lines (bottom panel) of the $T_{\mathrm{mw}} - M$ cluster scaling relation for the C (triangles, solid line), D4 (diamonds, triple-dot-dashed line), D3 (squares, short-dashed line), D2 (circles, dashed line) and D1 (crosses, dot-dashed line) simulation models. Colour bands are best fit errors to the cluster distributions at each redshift. The shaded area in the bottom panel is the rms dispersion of the normalisation fit for the cooling model.(see text for details)

clude data points above z=1 in the computation of β because cluster numbers drop rapidly (below 20) which, in some cases, causes large oscillations in the computed normalizations. Moreover in the case of the $L_X - M$ relation, the evolution of $y_0(z)$ with redshift appears to deviate from a straight line above $z \simeq 1$. In Table 2 we provide a complete list of the $\log A$, β and α fitting parameters and associated statistical errors for all scalings and cooling models investigated in this paper. The displayed values are valid in the redshift range $0 < z < 1$. In the top and middle panels the coloured bands correspond to the $\pm 1\sigma$ envelope of the best fit errors obtained at each redshift for α, and $\log y_0$. The shaded area in the bottom panels are r.m.s. fit dispersions of the normalisations, $\log y_0$, computed for the cooling model using Eq. (17).

Results from different simulation runs are coded in the following way: triangles and solid lines stand for the cooling model, diamonds and triple-dot-dashed lines represent the D4 model, squares and short-dashed lines are for D3 model,
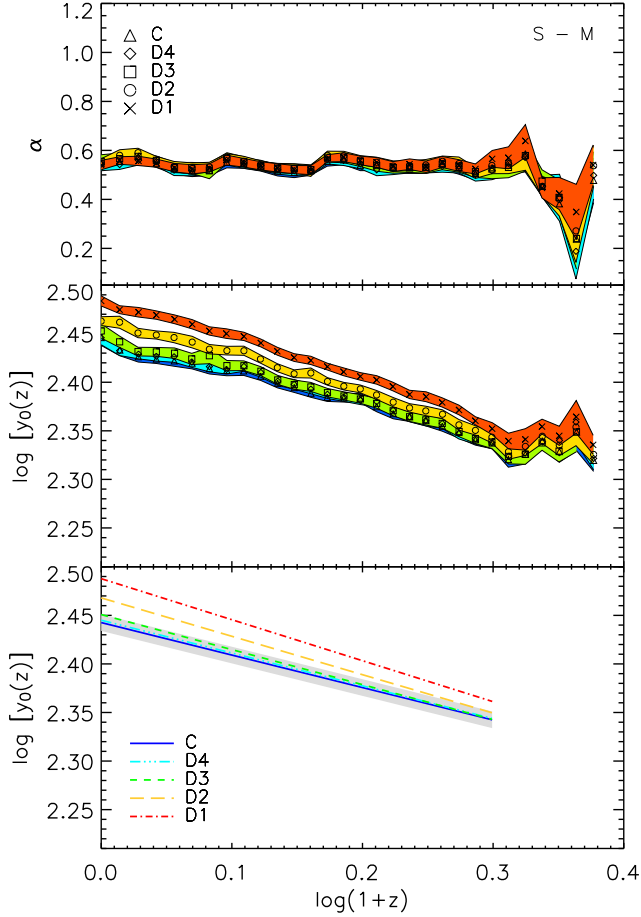
Figure 4. Evolution of the slope (top panel), normalisation (middle panel), and normalisation best fit lines (bottom panel) of the $S - M$ cluster scaling relation for the C, D4, D3, D2, D1 simulation models. Symbols, lines and colours are the same as in Fig 3.

Figure 5. Evolution of the slope (top panel), normalisation (middle panel), and normalisation best fit lines (bottom panel) of the $Y - M$ cluster scaling relation for the C, D4, D3, D2, D1 simulation models. Symbols, lines and colours are the same as in Fig 3.

circles and dashed lines for the D2 models and crosses and dot-dashed lines are for the D1 model. Here we have omitted the D5 model for clarity. It provides the same fitting results as the cooling model. This confirms expectations and the comments made in the last paragraph of Section 2.3.

The top panels of these Figures allow us to conclude that the α slopes of our scalings are fairly insensitive to dust cooling. These also show no evidence of systematic variations with redshift for all scalings, which is an important requirement when fitting the cluster distributions with power-laws of the form Eqs. (11)-(14). The redshift independence of the slopes with the dust model confirms our findings at redshift zero. The scatter (non-systematic "oscillations") at high redshift is caused by the decrease of the number of clusters with $M_{\rm lim} \geqslant 5 \times 10^{13} h^{-1} M_\odot$, the sample selection used for all fits.

The main effect of cooling by dust is reflected in the changes it produces in the normalisations of the cluster scaling laws. Again, the the impact of dust is different depending on the scaling under consideration. For the $T_{\rm mw} - M$ scaling in Fig. 3 we see a sytematic variation with the dust model (ordered in the following way: C, D4, D3, D2, D1), but differences between models are within the errors and fit
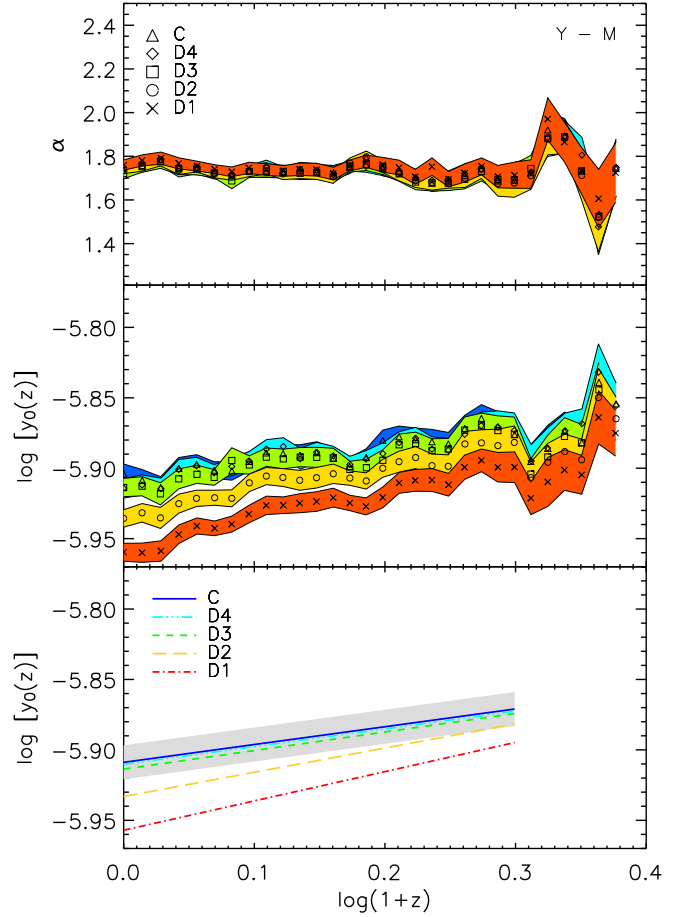
dispersions of each others. For the evolution of the normalisations of the $S - M$, $Y - M$, and $L_{\rm X} - M$ scalings (see Figs. 4, 5, and 6) we conclude that the inclusion of dust cooling causes significant departures from the standard radiative cooling model depending on the dust model parameters. For example, this is clear from the non-overlapping errors and fit dispersions of the normalisations for the D2 and D1 models. For all scalings, the relative strength of the effect of dust follows the relative intensity of the cooling functions presented in Section 2.3. This orders the models in the following way: C, D4, D3, D2, D1 with increasing normalisations for the $T_{\rm mw} - M$ and $S - M$ scalings and decreasing normalisations for the $Y - M$ and $L_X - M$ relations.

We end this section by noting that we find positive evolution (relative to the expected self-similar evolution, i.e. for a given x in Eq (15) the property yf is higher at higher redshifts) for the $Y - M$ and $L_X - M$ (models D1 and D2 only) relations whereas the $T_{\rm mw} - M$, and $S - M$ relations show negative evolutions relative to the self-similar model. This is in line with the findings from simulations with radiative cooling of similar size and cosmology, see eg (da Silva et al. 2004; Aghanim et al. 2008).
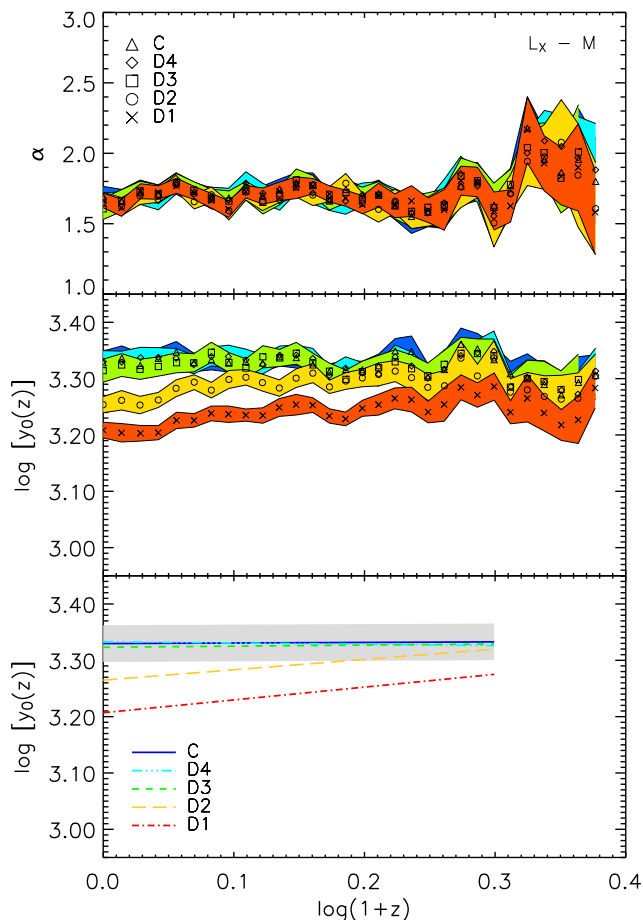
Figure 6. Evolution of the slope (top panel), normalisation (middle panel), and normalisation best fit lines (bottom panel) of the $L_X - M$ cluster scaling relation for the C, D4, D3, D2, D1 simulation models. Symbols, lines and colours are the same as in Fig 3.

6   DISCUSSION

6.1   Efficiency of the dust cooling

In agreement with the cooling functions of (Montier & Giard 2004), the dust cooling is most effective in the cluster temperature regime. The relative importance of the dust cooling with respect to the gas radiative cooling is strongly dependent on the dust abundances and the intrinsic physical properties of the dust. This is clearly shown in our scaling relations results:

- the $T_{\mathrm{mw}} - M$ relation is almost unchanged when adding dust cooling to the radiative gas cooling (see Fig. 3). Our results show that the (mass weighted) temperature–mass relation within R_{200}, is essentially driven by the gravitational heating of the gas (due to its infall on the cluster potential well), and that the physics of baryons (at least for the physics implemented in the simulations presented in this paper) play very little role in the outer parts of halos which dominate the estimation of the mass-weighted temperature and integrated mass. Since gas cooling tends to disturb the dark matter distribution at the centre of clusters in high resolution simulations (Gnedin et al. 2004), the cooling by dust may amplify this effect, and thus modify scaling rela-

tions like the $T_{\mathrm{mw}} - M$. In the case of observationally derived quantities, scaling laws will be drawn from overall quantities that will proceed from mixed-projected information over a wide range of radii. If a gradient exist in the dust effect towards the cluster centre, an "overall" temperature might bear the signature of the structural effect of dust. Anyway this quantification is beyond the scope of this paper and will be investigated in a forthcoming paper. There is also no significant effect between the different dust models and the radiative case on the evolution of the slope and normalisation of the $T_{\mathrm{mw}} - M$ relation.

- On the other hand the other three scaling laws are deeply related to the clusters baryonic component. The clear effect on the $S - M$, $Y - M$, and $L_X - M$ relations illustrates this fact (see Figs. 4, 5, and 6). We found that the slopes of these scalings remain fairly insensitive to dust, whereas normalisations show significant changes depending on the dust parameters. Relative changes in the normalisations at redshift zero and $M_0 = 10^{14} h^{-1} \mathrm{M}_\odot$ can be as high as 25% for $L_X - M$ and 10% for the $S - M$, $Y - M$ relations for the D1 model. Models with lower dust abundances and MRN grain size distributions present smaller but systematic variations relative to the C model. As any other cooling process, the cooling due to dust tends to lower the normalisations of the $Y - M$, and $L_X - M$ scalings due to the decrease of the hot gas fractions and densities which dominate the increase of temperature. The increase of normalisations for the $S - M$ and $T_{\mathrm{mw}} - M$ relations with added dust cooling is also in line with expectations because cooling converts cold, dense, gas into collisionless star forming material, which raises the mean temperature and entropy of the remaining gas.

- Our simulations allow us to quantify the relative impact of the dust parameters on the investigated cluster scalings (see Figs. 3 to 6 and Table 2). From one model to another one can identify two clear effects due to dust: (i) it shows the expected effect of the dust abundance, which from models D4 to D2 raise by a factor of 10, producing a change of normalisations relative to the purely radiative case (model C), from almost zero percent contribution to about 14%, 5% and 6% contributions for the $L_X - M$, $Y - M$ and $S - M$ relations, respectively. (ii) Even more striking is the effect of the intrinsic dust grain physical properties. The variation of normalisations relative to the C model, change from a zero percent level for model D4 to about 25% ($L_X - M$) and 10% ($Y - M$, and $S - M$) for the model D1 (ie the relative change from models D2 to D1 is about 13% and 5%, respectively). All these percentages were calculated using normalisations at redshift zero and $M_0 = 10^{14} h^{-1} \mathrm{M}_\odot$. Therefore the size of the grains comes to be an equally important parameter varying the efficiency of the dust cooling. The smaller the grain, the stronger the cooling.

- From Figs. 3, 4, 5, and 6 one finds that differences between normalisations become progressively important with decreasing redshift. This confirms expectations because metallicity was modelled in simulations as a linearly increasing function of time. Although our implementation of metallicity should only be regarded as a first order approximation to the modelling of more complex physical processes (acting on scales below the resolution scale of the present set simulations), it would be interesting to investigate whether a similar effect remains (ie the effects of dust become progressively important at low redshift) when such processes

are taken into account throughout the formation history of galaxy clusters (see discussion below).

6.2   Limitation of the dust implementation

In order to implement the presence of dust in the numerical simulations, we chose a "zero order approach": we directly correlated the presence of dust with the presence of metals under the assumption that there is no segregation in the nature of the material withdrawn from galaxies and injected in the IGM/ICM (metals, gas, stars or dust). However, this assumption suffers from limitations linked to the dust lifetime. Indeed, dust grains strongly suffer of sputtering and within their lifetime they are depleted from metals which, contrary to dust grains, are not destroyed i.e. remain in the ICM/IGM. Therefore our whole analysis is to be considered within the framework of this assumption, and is to be understood as a basic implementation of the effects of dust with the objective of assessing whether dust has a significant impact on large scale structure formation, and consequently to quantify these effects at first order.

Moreover, our implementation is also *ad hoc*. Indeed, beside the cooling function of dust, our implementation is not a physical implementation. We did not deal *stricto senso* with the physics of the dust creation and dust destruction processes. This would be a step further, and is yet beyond the scope of this paper as mentioned above. However, making use of the cooling function by (Montier & Giard 2004), we have performed a fully self-consistent implementation of the effect of dust as a cooling vector of the ICM/IGM. Indeed, on the basis of the cooling function, the implementation encapsulates the major physical processes to which dust is subjected and acts as a non-gravitational process at the scale of the ICM and the IGM.

As already mentioned, we directly correlated the abundance of dust with metallicity, thus to the metallicity evolution, which chosen evolution law is quite drastic: $Z = 0.3(t/t_0)Z_\odot$. Indeed, if the metallicity at $z = 0$ is normalized to the value of $0.3Z_\odot$, it is lowered to ~ 0.2 at $z = 0.5$ and ~ 0.1 at $z = 1$. However, other numerical works based on simulations including physical implementation of metal enrichment processes but without dust agree well with observational constraints (mainly provided by X-ray observations of the Fe-K line) which indicate high metalicity values, $Z \sim 0.3Z_\odot$, up to redshifts above 1.0 (Cora et al. 2008; Borgani et al. 2008). This shows that, as for the stellar component which is already in place in galaxies when clusters form, the metal enrichment of the ICM/IGM has occured through the feedback of galaxy formation and evolution, and therefore it *de facto* strongly enriched the IGM/ICM bellow $z = 1$. It also might give hints that the high metallicity of clusters could be correlated to the dust enrichment of the IGM/ICM. Indeed, the amount of gaseous iron in galaxies such as the Milky Way is $\sim 0.01Z_\odot$. An early enrichment of dust in the IGM and/or the ICM, which once sputtered will provide metals, could explain part of the iron abundances found in the ICM at low redshifts. This hypothesis seems to be consolidated by the few works that have investigated dust as a source for metals in the material stripped from galaxies via dynamical removal within already formed clusters (Aguirre et al. 2001) or via an early IGM enrichment

at high redshift during the peak of star formation around $z = 3$ (Bianchi & Ferrara 2005). The latter work stressed that only big grains ($a > 0.1\mu$m) can be transported on a few 100kpc physical scale, however leading to a very inhomogenous spatial enrichment in metals once the dust grains are sputtered. For all these reasons, by underestimating the metallicity at high redshifts, we might have underestimated the amount of dust injected in the ICM at high redshift, and thus the efficiency of dust cooling when integrated from early epoch down to redshift zero

7   CONCLUSION

In this work, we have presented the first simulations of structure formation investigating the effect of dust cooling on the properties of the intra-cluster medium. We have compared simulations with radiative *plus* dust cooling with respect to a purely radiative cooling simulation. We have shown that:

• The cooling due to dust is effective at the cluster regime and has a significant effect on the "baryon driven" statistical properties of cluster such as $L_X - M$, $Y - M$, $S - M$ scaling relations. As an added non-gravitational cooling process dust changes the normalisation of these laws by a factor up to 27% for the $L_X - M$ relation, and up to 10% for the $Y - M$ and $S - M$ relations. On the contrary, dust has almost no effect on a "dark matter driven" scaling relation such as the $T_{mw} - M$ relation.

• The inclusion of cooling by dust does not change significantly the slopes of the cluster scaling laws investigated in this paper. They compare with the results obtained in the radiative cooling simulation model.

• Through the implementation of our different dust models, we have demonstrated that the dust cooling effect at the scale of clusters depends strongly on the dust abundance in the ICM, but also on a similar proportion on the size distribution of dust grains. Therefore the dust efficiency is strongly dependent on the nature of the stripped and ejected galactic material, as well as the history of these injection and destruction processes along the cluster history. Indeed the early enrichment of dust might provide an already modified thermodynamical setup for the "to-be-accreted" gas at lower redshifts.

The setup of our simulations and the limitation of our dust implementation can be considered at a "zero order" test with which we demonstrated the active effect of dust on structure formation and especially at the cluster scale. In order to go one step further, a perspective of this work will be needed to couple the radiative cooling function of dust with a physical and dynamical implementation of the creation and destruction processes of dust in the IGM/ICM.

REFERENCES

Aghanim, N., da Silva, A. C., Nunes, N., 2008, submitted to A&A, astro-ph/0808.0385

Aguirre, A., Hernquist, L., Schaye, J., Katz, N., Weinberg, D., and Gardner, J. 2001, ApJ 561, p521

Arnaud, M. 2005, Background Microwave Radiation and Intracluster Cosmology, 77 (astroph/0508159)

Bai, L., Rieke, G., Rieke, M., Hinz, J., Kelly, D., and Blaylock, M. 2006, ApJ 639, p827

Bai, L., Marcillac, D., Rieke, G., Rieke, M., Tran, K., Hinz, J., Rudnick, G., Kelly, D., and Blaylock, M. 2007, ApJ 664, p181

Bardeen, J. M., Bond, J. R., Kaiser, N., & Szalay, A. S., 1986, ApJ, 304, 15

Bianchi, S., & Ferrara, A. 2005, MNRAS, 358, 379

Borgani, S., Fabjan, D., Tornatore, L., Schindler, S., Dolag, K., & Diaferio, A. 2008, Space Science Reviews, 134, 379

Cattaneo, A., & Teyssier, R. 2007, MNRAS, 376, 1547

Chelouche, D., Koester, B. P., & Bowen, D. V. 2007, ApJ (Lett.), 671, L97

Cora, S. A., Tornatore, L., Tozzi, P., & Dolag, K. 2008, MNRAS, 386, 96

Conroy, C., & Ostriker, J. P. 2007, ArXiv e-prints, 712, arXiv:0712.0824

Conroy, C., Wechsler, R. H., & Kravtsov, A. V. 2007, ApJ, 668, 826

Couchman, H. M. P., 1991, Ap.J, 368, L23

Couchman H. M. P., Thomas P. A., Pearce F. R., 1995, MNRAS, 452, 797

Domainko, W., et al. 2006, A&A, 452, 795

Draine, B. T., & Salpeter, E. E. 1979, ApJ, 231, 77

Dwek, E. 1981, ApJ, 247, 614

Dwek, E., Rephaeli, Y., & Mather, J. C. 1990, ApJ, 350, 104

Eke, V. R., Navarro, J. F., & Frenk, C. S., 1998, ApJ, **503**, 569

Giard, M. et al., 2008, accepted for publication in A&A

Gnedin, O. Y., Kravtsov, A. V., Klypin, A. A., & Nagai, D. 2004, ApJ, 616, 16

Kaiser N., 1986, MNRAS, 222, 323

Kapferer, W., et al. 2006, A&A, 447, 827

Krick, J. E., & Bernstein, R. A. 2007, Astron. J., 134, 466

Loewenstein, M. 2006, ApJ, 648, 230

Mathis, J. S., Rumpl, W., & Nordsieck, K. H. 1977, ApJ, 217, 425

McNamara, B. R., & Nulsen, P. E. J. 2007, Ann. Rev. Astron. Ap., 45, 117

Moll, R., et al. 2007, A&A, 463, 513

Montier, L., and Giard, M. 2004, A&A 417, p401

Montier, L., and Giard, M. 2005, A&A 439, p35

Muanwong, O., Thomas, P.A. Kay, S.T., Pearce, F.R., Couchman, H.M.P., 2001, ApJ, 552, L27.

Muanwong O., Thomas P. A., Kay S. T., Pearce F. R., 2002, MNRAS, 336, 527

Muanwong, O., Kay, S.T., Thomas, P.A. 2006, ApJ,649, 640.

Muller, S., Wu, S.Y., Hsieh, B.C., Gonzalez, R., Loinard, L., Yee, H., Gladders, M. 2008, acepted for publication in ApJ, arXiv:0801.2613

Murante, G., et al. 2004, ApJ (Lett.), 607, L83

Murante, G., Giovalli, M., Gerhard, O., Arnaboldi, M., Borgani, S., & Dolag, K. 2007, MNRAS, 377, 2

Pearce F. R., Couchman H. M. P., 1997, New Astronomy, 2, 411

Pearce F. R., Thomas P. A., Couchman H. M. P., Edge A. C., 2000, MNRAS, 317, 1029

Popescu, C., Tuffs, R., Fischera, J., and Völk, H. 2000 A&A 354, p480

Sarazin, C. L. 1988, Cambridge Astrophysics Series, Cambridge: Cambridge University Press, 1988,

da Silva, A.C., Kay, S.T., Liddle, A.R., Thomas, P.A. 2004, MNRAS, 348, 1401

Springel, V., & Hernquist, L. 2003, MNRAS, 339, 312

Stickel, M., Lemke, D., Mattila, K., Haikala, L.K. and Klaas, M. 1998, A&A 329, p55

Stickel, M., Klaas, U., Lemke, D., and Mattila, K. 2002, A&A 383, p367

Sugiyama, N., 1995, Astrophys.J.Suppl., 100, 281

Sutherland R. S., Dopita M. A., 1993, ApJ Suppl., 88, 253

Thacker R. J., Couchman H. M. P., 2000, ApJ, 545, 728

Thomas P. A., Couchman H. M. P., 1992, MNRAS, 257, 11

Thomas P. A. et al. (the Virgo Consortium), 1998, MNRAS, 296, 1061

Voit, G. M. 2005, Reviews of Modern Physics, 77, 207

Weingartner, J., Draine, B. T. and Barr, D. 2006 ApJ, 645, p1188

This paper has been typeset from a TeX/ LaTeX file prepared by the author.

Table 2. Best fir values of the parameters α, $\log A$ and β as well as their respective 1σ errors. These values are valid within the redshift range $0 < z < 1$.

	Model C	Model D5	Model D4	Model D3	Model D2	Model D1
$T_{\mathrm{mw}} - M$						
α_{TM}	0.61 ± 0.02	0.61 ± 0.02	0.61 ± 0.02	0.62 ± 0.02	0.63 ± 0.02	0.63 ± 0.02
$\log A_{\mathrm{TM}}$	0.195 ± 0.002	0.195 ± 0.003	0.196 ± 0.002	0.197 ± 0.003	0.201 ± 0.002	0.204 ± 0.002
β_{TM}	-0.14 ± 0.01	-0.14 ± 0.01	-0.14 ± 0.01	-0.15 ± 0.01	-0.16 ± 0.01	-0.16 ± 0.01
$S - M$						
α_{SM}	0.55 ± 0.03	0.54 ± 0.03	0.54 ± 0.03	0.56 ± 0.03	0.55 ± 0.02	0.54 ± 0.02
$\log A_{\mathrm{SM}}$	2.443 ± 0.002	2.444 ± 0.002	2.445 ± 0.002	2.451 ± 0.002	2.468 ± 0.002	2.488 ± 0.02
β_{SM}	-0.33 ± 0.01	-0.34 ± 0.01	-0.34 ± 0.01	-0.36 ± 0.01	-0.40 ± 0.01	-0.42 ± 0.01
$Y - M$						
α_{YM}	1.74 ± 0.03	1.72 ± 0.03	1.73 ± 0.03	1.72 ± 0.02	1.74 ± 0.02	1.76 ± 0.02
$\log A_{\mathrm{YM}}$	-5.909 ± 0.002	-5.907 ± 0.002	-5.910 ± 0.002	-5.914 ± 0.002	-5.933 ± 0.002	-5.957 ± 0.002
β_{YM}	0.12 ± 0.01	0.11 ± 0.01	0.13 ± 0.02	0.13 ± 0.01	0.17 ± 0.01	0.21 ± 0.01
$L_{\mathrm{X}} - M$						
α_{LM}	1.69 ± 0.07	1.68 ± 0.07	1.65 ± 0.07	1.61 ± 0.08	1.67 ± 0.05	1.67 ± 0.05
$\log A_{\mathrm{LM}}$	3.330 ± 0.006	3.334 ± 0.006	3.333 ± 0.005	3.323 ± 0.005	3.265 ± 0.005	3.207 ± 0.004
β_{LM}	0.01 ± 0.03	-0.02 ± 0.03	-0.02 ± 0.03	0.02 ± 0.03	0.18 ± 0.03	0.23 ± 0.03